The Plant Cell, Vol. 15, 612–625, March 2003, www.plantcell.org © 2003 American Society of Plant Biologists

Cell Polarity and PIN Protein Positioning in Arabidopsis Require *STEROL METHYLTRANSFERASE1* Function

Viola Willemsen,[a] Jirí Friml,[b,1] Markus Grebe,[a] Albert van den Toorn,[a] Klaus Palme,[c] and Ben Scheres[a,2]

[a] Developmental Genetics, Utrecht University, Padualaan 8, 3584 CH, Utrecht, The Netherlands
[b] Max-Delbrück-Laboratorium in der Max-Planck-Gesellschaft, Carl-von-Linné-Weg 10, 50829 Köln, Germany
[c] Institut für Biologie II, Zell-biologie, Universität Freiburg, 79104 Freiburg, Germany

Plants have many polarized cell types, but relatively little is known about the mechanisms that establish polarity. The *orc* mutant was identified originally by defects in root patterning, and positional cloning revealed that the affected gene encodes STEROL METHYLTRANSFERASE1, which is required for the appropriate synthesis and composition of major membrane sterols. *smt1*^{orc} mutants displayed several conspicuous cell polarity defects. Columella root cap cells revealed perturbed polar positioning of different organelles, and in the *smt1*^{orc} root epidermis, polar initiation of root hairs was more randomized. Polar auxin transport and expression of the auxin reporter *DR5*-β-glucuronidase were aberrant in *smt1*^{orc}. Patterning defects in *smt1*^{orc} resembled those observed in mutants of the *PIN* gene family of putative auxin efflux transporters. Consistently, the membrane localization of the PIN1 and PIN3 proteins was disturbed in *smt1*^{orc}, whereas polar positioning of the influx carrier AUX1 appeared normal. Our results suggest that balanced sterol composition is a major requirement for cell polarity and auxin efflux in Arabidopsis.

INTRODUCTION

Polarized cells distribute intracellular components asymmetrically along a particular axis. A polar distribution of factors can facilitate specialized cellular functions, such as absorption and secretion in epithelial cells (Rodriguez-Boulan and Nelson, 1989). Cell polarity also can provide positional information in multicellular pattern formation. In *Drosophila* and *Caenorhabditis elegans*, for example, localized membrane-tethered proteins guide asymmetric cell division to establish different daughter cells (Knoblich, 2001). One manifestation of plant cell polarity at the multicellular level is polar transport of the phytohormone auxin, which is important for various developmental processes, such as vascular patterning, tropism, shoot development, and axis formation (Estelle, 1998). In Arabidopsis, the cloning of genes defective in these processes has led to the identification of the PIN family of proteins implicated in auxin efflux (Chen et al., 1998; Gälweiler et al., 1998; Luschnig et al., 1998; Müller et al., 1998; Friml et al., 2002a, 2002b) and the AUX1 protein required for influx (Marchant et al., 1999; Rahman et al., 2001). PIN and AUX1 proteins are localized asymmetrically in several cell types; thus, they serve as molecular markers for cell polarity (Gälweiler et al., 1998; Müller et al., 1998; Swarup et al., 2001; Friml et al., 2002a, 2002b).

Vesicle trafficking has been shown to be important for correct polar PIN and AUX1 protein localization (Steinmann et al., 1999; Grebe et al., 2002). In *gnom/emb30* mutant embryos, the coordinated polar localization of the PIN1 protein is not established properly, and the mutant embryos and seedlings display variable defects in cell and tissue polarity (Mayer et al., 1993; Vroemen et al., 1996; Steinmann et al., 1999). The *GNOM* (*GN*) gene encodes a brefeldin A (BFA)–sensitive guanosine nucleotide exchange factor (GEF) on ADP-ribosylation factor (ARF)–type small G-proteins, which are regulators of vesicle trafficking (Steinmann et al., 1999). PIN1 rapidly cycles in an actin-dependent manner between the plasma membrane and the endosomes (Geldner et al., 2001). Consistent with a role for ARF-GEFs in PIN1 localization, the vesicle-trafficking inhibitor BFA causes intracellular PIN1 accumulation (Steinmann et al., 1999) and inhibition of auxin efflux (Delbarre et al., 1998; Morris and Robinson, 1998). In addition, AUX1 localization is sensitive to BFA, and AUX1 is one of the components that mediate epidermal cell polarity, as reflected by the disturbed polar localization of root hair outgrowth from *aux1* epidermal cells (Grebe et al., 2002).

Studies of vesicle trafficking in animal epithelial cells have revealed that depletion of cholesterol, the main animal sterol, reduces the polar delivery of target proteins (Keller and Simons, 1998). These findings have led to sorting models that involve lipid-protein clusters, of which cholesterol is a major component (Brown and London, 2000). In plants, a connection between membrane sterol composition and cell polarity has not been reported previously. However, several sterols structurally related to cholesterol are present in plants, sitosterol being the most abundant (Patterson et al., 1993). Campesterol, the next abundant sterol, is a precursor of brassinosteroids, which are involved in the control of plant growth and development (Altmann, 1998; Clouse and Feldmann, 1999).

In this study, we describe the Arabidopsis *orc* mutant, which was isolated as a single allele in a screen for root-patterning

[1] Current address: Zentrum für Molekularbiologie der Pflanzen, Universität Tübingen, Auf der Morgenstelle 3, 72076 Tübingen, Germany.
[2] To whom correspondence should be addressed. E-mail b.scheres@bio.uu.nl; fax 31-30-2513655.
Article, publication date, and citation information can be found at www.plantcell.org/cgi/doi/10.1105/tpc.008433.

mutants. Map-based cloning revealed that the *orc* mutation represents an allele of the *STEROL METHYLTRANSFERASE1* (*SMT1*) gene (also referred to as *CEPHALOPOD* [*CPH*]), which encodes an enzyme required for appropriate sterol levels and that is involved in C-24 alkylation of sterols during sterol biosynthesis (Diener et al., 2000; Schrick et al., 2002). We report specific defects for *smt1*^{orc} in the polarization of several different cell types and in polar auxin transport. Consistent with a primary role of the *SMT1* gene in cell polarity, the efflux carriers PIN1 and PIN3 showed aberrant localization in *smt1*^{orc} mutants. Our data provide evidence that sterols are involved intimately in the establishment of plant cell polarity and suggest a link between sterol biosynthesis and efflux carrier positioning.

RESULTS

The *orc* Mutation Alters the C Terminus of SMT1

The *orc* mutant was identified as a single recessive allele in a large-scale screen for ethyl methanesulfonate mutants affected in root development from embryogenesis onward (Scheres et al., 1996). The *orc* mutation maps to a single locus on chromosome 5 (see below). The primary root length of *orc* was <20% of wild-type length, and lateral roots showed similar defects in growth. In mature *orc* plants, leaf size was reduced and multiple primary inflorescences arose simultaneously (Figure 1F, arrows) and showed a reduction in elongation (Figure 1G). Furthermore, *orc* flowers had reduced fertility, sepals of terminal flowers often had frayed edges (Figure 1H), and terminal siliques frequently were fused in triplets (Figure 1I).

To investigate the molecular basis of the *orc* mutation, we isolated the affected gene by map-based cloning (Figure 2). Fine-mapping experiments located the gene on chromosome 5 BAC MSH12 between positions 32,946 and 72,976 (Figure 2B). Using primers from this region, a transformation-competent artificial chromosome (TAC) vector library (Lui et al., 1993) was screened, and overlapping TACs were transformed into *orc* homozygotes. The full-size TAC K12A16 complemented *orc* seedlings, whereas a deleted version did not (Figures 2C and 2D). This confined the position of the gene to TAC K12A16 region MSH12.32946-72976. In open reading frame (ORF) MSH12.18, a G-to-A substitution was found at the splice acceptor site of exon 13. The expected size of the mRNA was 1285 bp, and reverse transcriptase–mediated PCR of *orc* RNA, with primers matching the first 30 bp downstream of the ATG and 30 bp upstream of the stop codon of the SMT1 mRNA, resulted in two products. Sequencing showed that the fragments were alternative splice products. In one case, the next G after substitution served as a splice acceptor, and in the other case, the intron was not spliced out, which resulted in fragments of 1284 and 1390 bp, respectively (Figure 2F). One variant is pre-

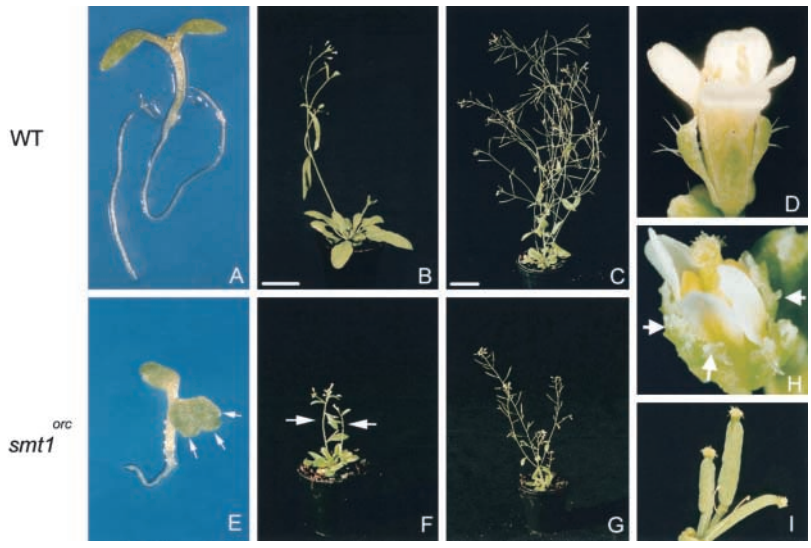

Figure 1. The *orc* Mutant Alters Plant Morphology.

(A) Five-day-old wild-type (WT) seedling grown on half-strength germination medium.
(B) Four-week-old wild-type plant.
(C) and **(D)** Six-week-old wild-type plant **(C)** and wild-type flower **(D)**.
(E) Five-day-old *orc* seedling grown on half-strength germination medium. Arrows indicate lobes of the cotyledons.
(F) Three-week-old homozygous *orc* plant with two primary inflorescences (arrows).
(G) Six-week-old homozygous *orc* plant.
(H) *orc* terminal flower with sepals with frayed edges (arrows).
(I) *orc* terminal flower with fused siliques.
Bars in **(B)** and **(C)** = 2.5 cm for **(B)**, **(C)**, **(F)**, and **(G)**.

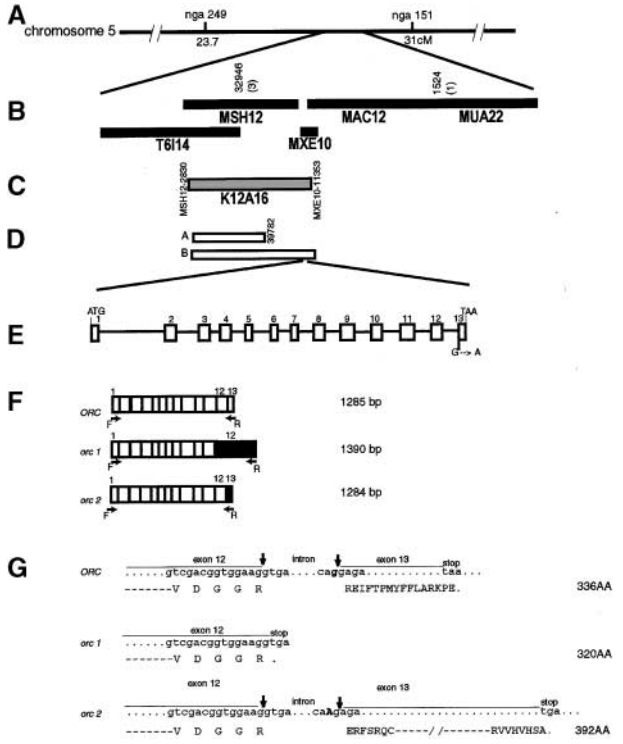

Figure 2. The *orc* Mutation Resides in the C-24 *SMT1* Gene.

(A) The *orc* between markers nga 249 and nga 151 (positions in centimorgan).

(B) *orc* location relative to a contig of five BAC clones (T6I14, MSH12, MXE10, MAC12, and MUA22). Numbers above BACs indicate the positions of the markers corresponding to the recombination breakpoints. The number of recombinant seedlings between the marker and the *orc* locus are shown in parentheses.

(C) The full-size TAC that complements the *orc* mutant.

(D) Partial TAC clones used for complementation; only B was complementing.

(E) Structure of *SMT1*. White boxes represent exons. The nucleotide sequence change at the splice site is depicted.

(F) The mutation in the splice acceptor site yields two cDNAs: mt cDNA 1 (no splicing), the altered exon depicted with the large black box, and mt cDNA 2 (the next acceptor site used), indicated with a small black box. Horizontal arrows depict the positions of the primers used for reverse transcriptase–mediated PCR: F, forward; R, reverse (see Methods).

(G) Alternative splicing leads to an early stop and a truncated protein. Vertical arrows indicate the intron-exon boundaries.

dicted to introduce a stop codon, and a frame shift in the other variant leads to a truncated protein (Figure 2G).

A genomic HindIII fragment of 8.4 kb containing the MSH12.18 ORF, including its promoter but excluding neighboring ORFs, was cloned into a binary vector and transformed into *orc* homozygous plants. The introduced gene complemented all aspects of the *orc* mutant, and we concluded that the mutation in this ORF was responsible for the *orc* phenotype (data not shown). MSH12.18 encodes SMT1, which was cloned independently by Diener et al. (2000) and Schrick et al. (2002). SMT1 has been proposed to be involved in sterol biosynthesis via methyl additions that form campesterol and sitosterol, which are precursors of brassinosteroids and a major membrane component, respectively (Diener et al., 2000). The *smt1^{orc}* mutation carries the same lesion in SMT1 as the independently isolated Landsberg *erecta* allele *cph-GXIII* (Schrick et al., 2002), and despite the truncation of only the C-terminal part of the protein, which may suggest that these alleles are not null mutants, both profoundly affect sterol composition. In agreement with investigations of other *smt1* alleles, we detected a significant reduction of sitosterol and a significant increase of cholesterol in *smt1^{orc}*, whereas campesterol levels were largely unaffected (Table 1). Moreover, sitosterol, campesterol, stigmasterol, cholesterol, and epibrassinolide did not rescue the *smt1^{orc}* mutant phenotype (data not shown) (Diener et al., 2000; Schrick et al., 2002).

Cell Polarity Defects in *smt1^{orc}* Seedlings

In vertically grown wild-type seedlings, differentiated columella cells in tiers 2 through 4 have a polarized morphology, with starch-containing plastids (amyloplasts) at the basal ends (MacCleery and Kiss, 1999) (Figures 3A and 3B). When analyzing the *smt1^{orc}* phenotype at the cellular level, we noted cell polarity defects in columella root cap cells (Figures 3E and 3F). We determined the apical-basal (proximal-distal) polarity of the cells in *smt1^{orc}* in relation to the main root axis, and because cell shapes may vary in *smt1^{orc}* roots (Figure 3E) but no correlation was observed between cell shape and the disturbance of polarity markers, "straight" cells were preselected for statistical analysis (Table 2, Figures 4A to 4D). In these cells, we determined the mid plane of the cell and counted the percentage of amyloplasts that passed to the apical side to quantify the more random localization of amyloplasts in *smt1^{orc}* columella cells (Figures 3E and 3F, Table 2).

Whereas plastid location responds to gravity, the nucleus of wild-type columella cells is located at the apical end independent of the gravity vector (MacCleery and Kiss, 1999) (Figure 3C). To quantify the position of the nucleus in columella cells, a ratio was determined between the distance from the apical cell wall to the apical side of the nucleus and the cell length. In the wild type, the nuclei resided at the apical side of columella cells (ratio of 0 to 0.2), whereas in *smt1^{orc}* columella cells, the positions of the nuclei were found in a broader range (ratio of 0 to 0.6) (Figures 3G and 4A). The randomized positions of amyloplasts and nuclei in *smt1^{orc}* columella cells suggest that columella cells in *smt1^{orc}* mutants are defective in apical-basal polarity.

Table 1. Altered Sterol Composition in *smt1^{orc}* Plants

Sterol	Wild Type	*smt1^{orc}*
Sitosterol	73.9 ± 4.1	42.2 ± 1.6
Campesterol	18 ± 1.8	22.3 ± 0.3
Stigmasterol	2.3 ± 0.7	Trace
Cholesterol	2.2 ± 0.1	14.7 ± 1.5

Values represent percentages (±SD) of the total sterol content and are calculated from two independent sterol isolations and quantifications.

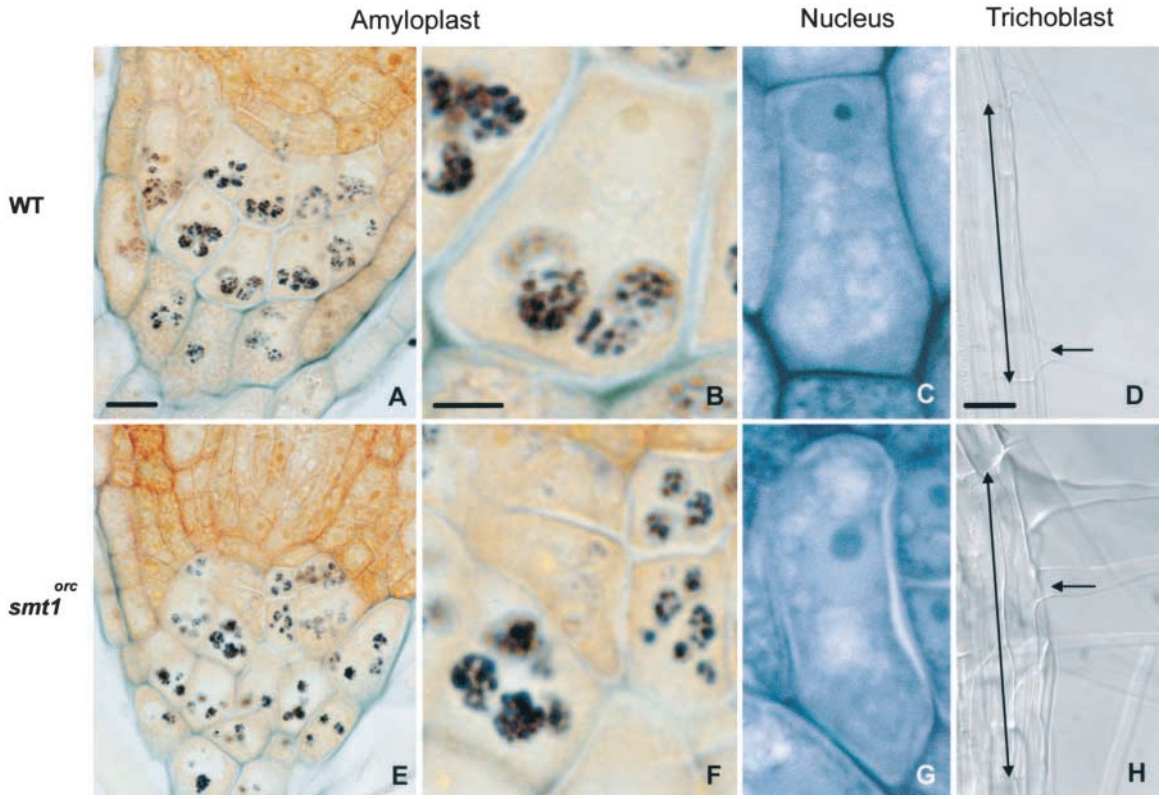

Figure 3. Cell Polarity Defects in *smt1*^{orc}.

(A) and **(B)** In the wild type (WT), amyloplasts are located at the basal ends of columella cells.
(C) The nucleus is located at the apical end.
(D) Root hairs initiate from the basal end of the polarized trichoblast.
(E) and **(F)** Amyloplast position in *smt1*^{orc} columella cells.
(G) Nuclear localization in *smt1*^{orc} columella cells.
(H) The initiation site of *smt1*^{orc} root hairs.
In **(D)** and **(H)**, long arrows indicate trichoblast length, and short arrows indicate the root hair initiation site. In **(A)** to **(C)** and **(E)** to **(G)**, plastic sections of 5-day-old seedling roots are shown; whole mounts are shown in **(D)** and **(H)** under Nomarski optics. Bars = 25 μm in **(A)** and **(E)**, 10 μm in **(B)** for **(B)**, **(C)**, **(F)**, and **(G)**, and 20 μm in **(D)** and **(H)**.

Another root cell type with conspicuous apical-basal polarity is the trichoblast, because hair initiation and outgrowth occur at its basal end (Figures 3D and 4B) (Massucci and Schiefelbein, 1994). Compared with the wild type, the initiation of hairs in the *smt1*^{orc} trichoblast was more randomized over the apical-basal axis (Figures 3H and 4B). The altered distribution of polarity markers in different cell types of the *smt1*^{orc} mutant suggests that the *SMT1* gene is required for polarity at the cellular level.

Application of the Synthetic Auxin 2,4-D Shifts *smt1*^{orc} Root Hairs Basally

The establishment of apical-basal trichoblast cell polarity involves the putative auxin influx carrier AUX1 and other factors sensitive to inhibitors of vesicle trafficking, which may include as yet unidentified efflux carriers (Grebe et al., 2002). To determine if defects in auxin influx cause trichoblast polarity abnormalities in *smt1*^{orc}, we applied the synthetic auxin 2,4-D, a preferential substrate for the auxin influx system, to the growth medium (Delbarre et al., 1996). Application of 20 nM 2,4-D to wild-type trichoblasts induced shifting of the root hair to the basal end of the cell (Figure 4C). *aux1* trichoblasts do not respond to this 2,4-D concentration (Grebe et al., 2002), but application of 20 nM 2,4-D to *smt1*^{orc} shifted root hairs basally to

Table 2. Quantification of Amyloplast Distribution in Columella Cells

Cell Type	Apical Amyloplasts[a]	No.[b]
Wild type	3.8 ± 0.7	536
smt1^{orc}	29.1 ± 1.8	493

[a] Percentage of amyloplasts (±SD) that had passed the median of the cell length to the apical side.
[b] Number of amyloplasts counted in two independent experiments.

almost the same position as in the wild type (Figure 4D). Thus, a perturbation of auxin influx does not appear to account for the epidermal polarity defects in *smt1*^{orc}; rather, a defect in response or the availability of auxin from endogenous sources seems to be the cause.

Aberrant Auxin Distribution and Defective Polar Auxin Transport in *smt1*^{orc}

We questioned whether auxin availability could be limited by a differential distribution in *smt1*^{orc}. The synthetic auxin-responsive reporter *DR5*-β-glucuronidase (*GUS*) (Ulmasov et al., 1997) is expressed in a polar transport–dependent manner in the distal root tip, and its expression correlates with high free auxin levels (Casimiro et al., 2001). Thus, *DR5-GUS* distribution in the embryo and root can be taken as an indicator of auxin distribution (Figures 5A and 5B) (Sabatini et al., 1999). *smt1*^{orc} embryos and seedlings were defective in the normal localization of the *DR5-GUS* maximum (Figures 5E and 5F). No consistent differences in *DR5-GUS* signal strength were observed in *smt1*^{orc}, indicating that auxin response levels are unaffected in the mutant.

When the synthetic auxin 2,4-D was applied externally, we observed high accumulation of *DR5-GUS* in the wild type at 5 μM 2,4-D (Figures 5C and 5D), whereas *smt1*^{orc} showed high accumulation already at 0.5 μM 2.4-D (Figures 5G and 5H). This finding confirms that auxin uptake is not reduced in *smt1*^{orc} root tips. Reporter activation upon application of lower concentrations of external 2,4-D may be explained by either more efficient uptake of 2,4-D or less efficient efflux in *smt1*^{orc}, resulting in the accumulation of exogenous auxin within root cells.

To investigate potential defects in polar auxin transport in *smt1*^{orc}, we applied ^{3}H-labeled indoleacetic acid (IAA, the major endogenous auxin) to the apical side of primary stem sections and measured the amount transported to the basal end. Polar auxin transport in stem sections is particularly sensitive to the action of the efflux carrier inhibitor napthylphthalamic acid (NPA) (Hertel et al., 1983; Heyn et al., 1987), which completely blocked transport in the wild type and *smt1*^{orc} (Figure 4E, column A). *smt1*^{orc} mutants displayed a 35% reduction in transport to basal stem segments compared with the wild type, which led, as expected, to an accumulation of ^{3}H-IAA in the apical segment (Figure 4F). A reduced number of vascular connections in the stem might affect auxin transport capacity, but the number of vascular bundles in cross-sectional areas of *smt1*^{orc} stem segments (5.9 ± 1.1, $n = 15$) was comparable to that in the wild type (6.7 ± 1.3, $n = 15$) (Figures 6A and 6D). Our data suggest that differences in auxin distribution occur in *smt1*^{orc} roots. Furthermore, these differences appear to be attributable not to decreased auxin influx or response but to decreased efflux capacity, which is consistent with the observed reduction of polar auxin transport in stem sections.

Mislocalized Auxin Reporter Expression in *smt1*^{orc} Correlates with Patterning and Growth Defects

Changes in auxin distribution reflected by *DR5-GUS* expression have been shown to correlate with patterning defects in

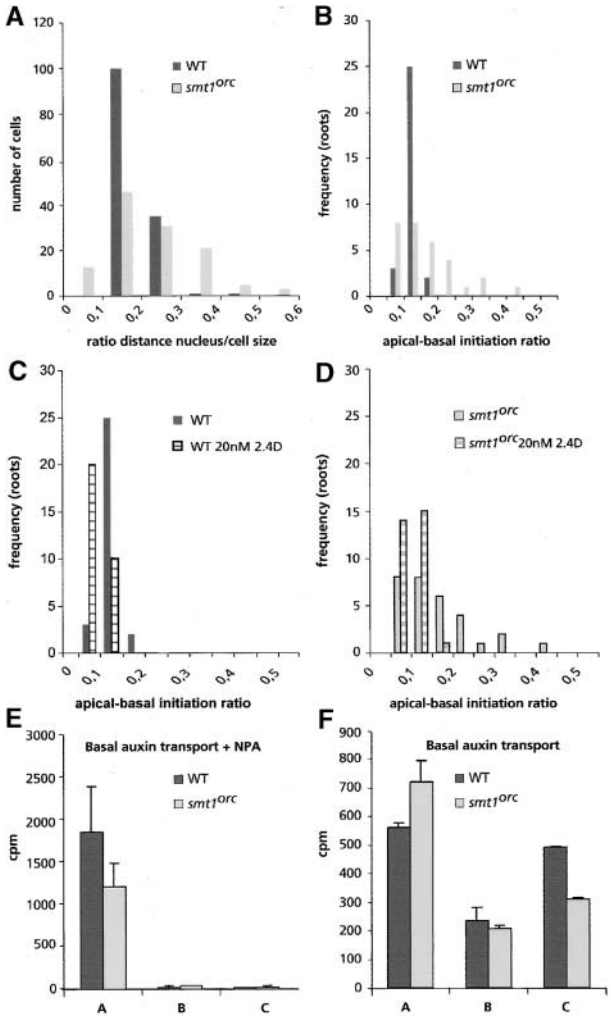

Figure 4. Quantification of Polarity Defects in *smt1*^{orc}.

(A) Positions of nuclei in columella cells of the wild type (WT) and *smt1*^{orc}. The relative position is the ratio between the distance from the apical cell wall to the apical side of the nucleus and the cell size. In the wild type, the nucleus is positioned toward the apical side (0, apical end; 1, basal end).

(B) to **(D)** Root hair initiation sites on trichoblasts of the wild type and *smt1*^{orc} are indicated in frequency distributions of average hair initiation per root (30 roots, 5 trichoblasts per root). Apical-basal initiation ratios indicate relative positions of hair initiation. Wild-type root hairs are located toward the basal end (0, basal end [normal end]; 1, apical end).

(B) Results in wild-type and *smt1*^{orc} seedlings germinated and grown for 5 days on half-strength germination medium.

(C) Results in wild-type seedlings germinated and grown for 5 days with and without 20 nM 2,4-D.

(D) Results in *smt1*^{orc} seedlings germinated and grown for 5 days with and without 20 nM 2,4-D.

(E) and **(F)** Polar auxin transport in stem sections. Results of polar auxin transport measurements were obtained from two independent experiments each on primary stem segments of 20 plants.

(E) Results in stem segments loaded with ^{3}H-IAA in the presence 2×10^{-6} M of the polar auxin transport inhibitor NPA at the apical side. Radioactivity was detected after transport and cutting in three sections: apical (column A), middle (column B), and basal (column C).

(F) As in **(E)** but without NPA.

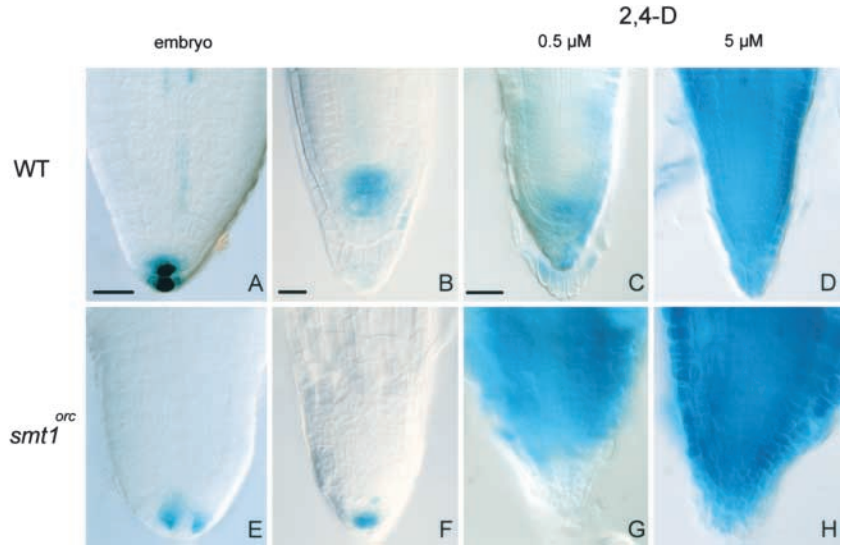

Figure 5. *DR5-GUS* Distribution Indicates Altered Auxin Distribution in *smt1*^{orc}.

(A) *DR5-GUS* distribution in a wild-type (WT) mature embryo.
(B) A maximum of *DR5-GUS* expression localizes to a wild-type columella root cap of a 5-day-old seedling.
(C) and **(D)** *DR5-GUS* staining after the application of 0.5 and 5 μM 2,4-D, respectively, in 5-day-old wild-type seedlings.
(E) Localization of *DR5-GUS* in a mature *smt1*^{orc} embryo.
(F) Localization of *DR5-GUS* in a *smt1*^{orc} root.
(G) and **(H)** *DR5-GUS* accumulation in *smt1*^{orc} roots treated with 0.5 and 5 μM 2,4-D, respectively.
Bars = 25 μm in **(A)** for **(A)** and **(E)**, 50 μm in **(B)** for **(B)** and **(F)**, and 75 μm in **(C)** for **(C)**, **(D)**, **(G)**, and **(H)**.

the root (Sabatini et al., 1999), and *smt1*^{orc} was identified originally as a root-patterning mutant (Scheres et al., 1996). Therefore, we analyzed the cellular organization of *smt1*^{orc} roots in some detail. Cell shapes and sizes in the proximal meristems of *smt1*^{orc} roots can be abnormal as a result of changes in the orientation of cell division, but epidermal, ground tissue, and vascular cells all were present (Figures 6B and 6E). In the distal root region, columella root cap cells were irregular in shape and alignment, but they expressed columella markers (Figures 6C, 6F, 6G, 6H, 6J, and 6K). Notably, cells with the characteristic morphology of the quiescent center (QC) were not observed in *smt1*^{orc} roots, and *smt1*^{orc} seedlings did not express the strictly QC-specific promoter trap line QC46 (Figures 6I and 6L) (Sabatini et al., 1999). Occasionally, cells in the position at which the QC would be expected expressed a columella root cap marker (Figure 6K). Furthermore, a 49% reduction in meristem size (measured as the region of mitotically active cells enclosed by the lateral root cap) compared with that in the wild-type meristem was observed in 6-day-old *smt1*^{orc} seedlings (n = 54). Thus, a full-size meristem cannot be maintained in *smt1*^{orc}. Defective meristem maintenance and the absence of a QC are in agreement with a function for the QC in stem cell maintenance (van den Berg et al., 1997).

In wild-type embryos, the hypophyseal cell divides to give rise to a small lens-shaped cell, the progenitor of the QC (Figure 7A, asterisks) (Dolan et al., 1993). In *smt1*^{orc}, the divisions of the hypophyseal cell were either absent (Figures 7I, 7K, and 7L, Table 3) or irregular (Table 3). Furthermore, *smt1*^{orc} embryos invariably lacked QC46 expression, which marks the wild-type QC from the heart stage onward (data not shown). In wild-type embryos, the basal cell of the ground tissue layer did not divide periclinally (Figures 7A, 7C, and 7D, Table 4). Postembryonically, repression of this division to maintain the basal stem cells of the ground tissue requires a functional QC (van den Berg et al., 1997). Consistent with a defective specification of QC identity, the basal stem cells of the ground tissue in late *smt1*^{orc} embryos frequently divided periclinally (Figures 7E, 7G, and 7H, arrow, Table 4).

We noted that cotyledons of wild-type embryos displayed a *DR5-GUS* maximum at the distal tip and lower expression in vascular cells (Figure 8A). By contrast, multiple *DR5-GUS* maxima occurred in *smt1*^{orc} embryonic cotyledons (Figure 8F). Most *smt1*^{orc} embryos showed abnormally shaped cotyledon primordia, and 19% (n = 57) of *smt1*^{orc} heart-stage embryos had more than two cotyledon primordia (Figure 7J, arrowheads). Therefore, the multiple *DR5*::*GUS* maxima in cotyledons of *smt1*^{orc} embryos correlate with defects in patterning.

Consistent with these defects, cotyledons of *smt1*^{orc} seedlings were lobed and often supernumerary (Figure 1E). The positions of lobes on cotyledons correlated with the venation pattern, because each lobe contained a primary vein with discontinuous vascular strands, as reported for other mutants with defects in vascular patterning (Figure 8G) (Przemeck et al., 1996; Deyholos et al., 2000; Carland et al., 2002). Frequently, isolated clusters of xylem elements (vascular islands) were formed in *smt1*^{orc} (Figure 8H), like those observed after the ap-

plication of polar transport inhibitors (Mattsson et al., 1999; Sieburth, 1999).

Consistent with the notion that auxin distribution influences not only patterning but also root tropism, we observed an irregular orientation of *smt1*^{orc} seedling roots on vertical plates (Figures 8D and 8I), and *smt1*^{orc} seedlings responded more randomly to a 90° change of the gravity vector (Figures 8E and 8J).

PIN1 and PIN3 Proteins but Not HA::AUX1 Are Inappropriately Localized in *smt1*^{orc}

To understand the molecular basis of the cell polarity defects in relation to the altered auxin distribution and the polar auxin transport defects in *smt1*^{orc}, we performed immunolocalization of hemagglutinin-tagged AUX1 (HA::AUX1), PIN1, and PIN3.

In protophloem cells, the complementing HA::AUX1 protein resides at the apical side in wild-type seedlings (Swarup et al., 2001). *smt1*^{orc} mutants were crossed to *aux1-22 HA::AUX1* plants, and in the progeny, *smt1*^{orc} seedlings showed normal HA::AUX1 protein localization in relation to the root axis (Figures 9A and 9B). Note that cells with oblique apical walls still retained AUX1 protein at the apical membrane only (Figure 9B, arrow). The putative auxin efflux carrier PIN1 localized to the basal end of central vascular cells, including AUX1-expressing protophloem cells, and to the basal end and the internal lateral side of pericycle cells (Figure 9C) (Gälweiler et al., 1998). In sharp contrast to the wild type, we detected PIN1 protein at lateral sites of elongated central vascular cells in *smt1*^{orc}, which were axialized correctly in the direction of the root axis (Figures 9D and 9E, arrows). In the wild type, the putative efflux carrier PIN3 localized uniformly throughout the plasma membranes of tier-2 and -3 columella cells (Figure 9F) (Friml et al., 2002a), whereas in *smt1*^{orc}, PIN3 was not distributed uniformly in tier-2 and -3 columella cells (Figures 9G and 9H). We conclude that *smt1*^{orc} function is required for correct PIN1 and PIN3 plasma membrane localization but not for proper AUX1 plasma membrane localization.

Appropriate plasma membrane localization of PIN1 requires the GN ARF-GEF protein (Steinmann et al., 1999). We investigated possible interactions between *SMT1* and *GN*, because cell polarity defects, including PIN1 mislocalization in both mutants, implicate both genes in a similar process. All different classes of seedlings obtained from crosses were analyzed and genotyped (Table 5). Genotyped *smt1*^{orc} *gn*^{T391} double-mutant seedlings were slightly smaller than *gn* seedlings, had multiple and lobed cotyledons like *smt1*^{orc}, and lacked root and hypocotyl pattern elements like *gn*, indicating the additivity of several phenotypes (Figures 9I to 9K). The mutation that causes the *emb30-1/gn*^{T391} phenotype behaves as a functional null allele in a heterologous system (Busch et al., 1996; Mossessova et al., 1998), suggesting that SMT1 acts on seedling pattern and polarity in the absence of GN activity. We cannot exclude the possibility that the additivity of the seedling phenotypes results from effects unrelated to cell polarity. However, the multiple-cotyledon phenotype that we observed in *smt1*^{orc} and in the double mutant has been linked to defective polar auxin transport (see Discussion), which indicates that SMT1 affects this process independent of GN.

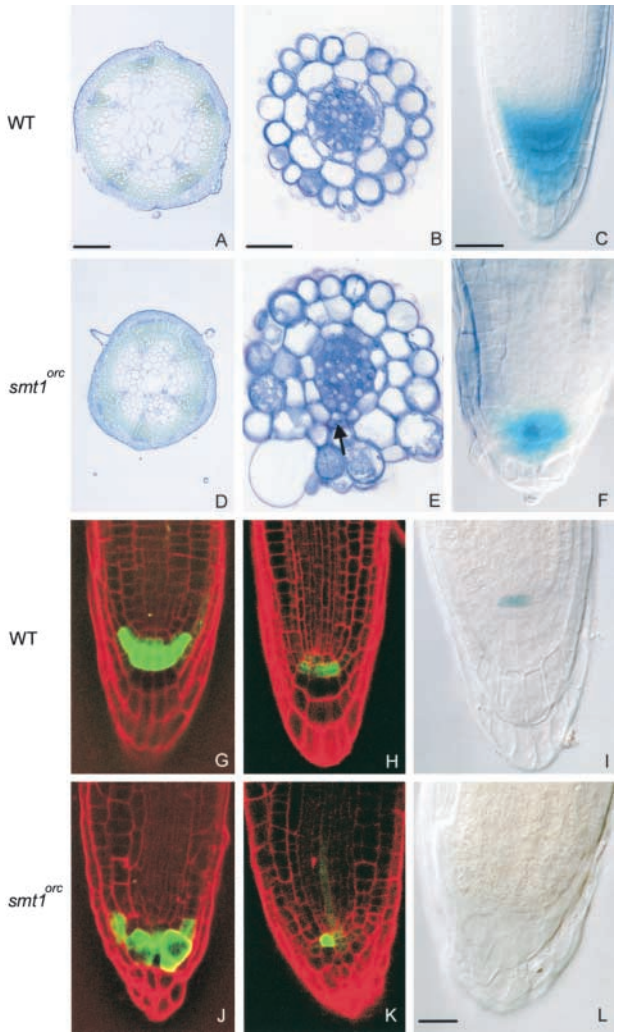

Figure 6. Defective QC Marker Expression and Organization of Columella Root Cap Cells in *smt1*^{orc}.

(A) Cross-section of a wild-type (WT) stem tissue used for polar auxin transport measurements.

(B) Regular radial organization of the root tip of a 5-day-old wild-type seedling.

(C) Columella-specific marker 35S-B2-GUS in a 5-day-old wild-type seedling.

(D) Cross-section of a *smt1*^{orc} stem tissue used for polar auxin transport measurements.

(E) Radial organization of a 5-day-old *smt1*^{orc} seedling with irregular cell shape. Extra division in the endodermis is indicated with the arrow.

(F) 35S-B2::GUS staining in a 5-day-old *smt1*^{orc} seedling.

(G) to **(I)** Columella-specific green fluorescent protein markers Q1630 **(G)** and J2341 **(H)** and the QC-specific promotor trap QC46 **(I)** in the wild type.

(J) to **(L)** Columella-specific green fluorescent protein markers Q1630 **(J)** and J2341 **(K)** and the QC-specific promotor trap QC46 **(L)** in *smt1*^{orc}.

(A), **(B)**, **(D)**, and **(E)** show toluidine blue–stained plastic sections; **(C)**, **(F)**, **(I)**, and **(L)** show Nomarski optic results after GUS staining; and **(G)**, **(H)**, **(J)**, and **(K)** show confocal laser scanning microscopy images. Bars = 200 μm in **(A)** for **(A)** and **(D)** and 50 μm in **(B)**, **(C)**, and **(L)** for all other panels.

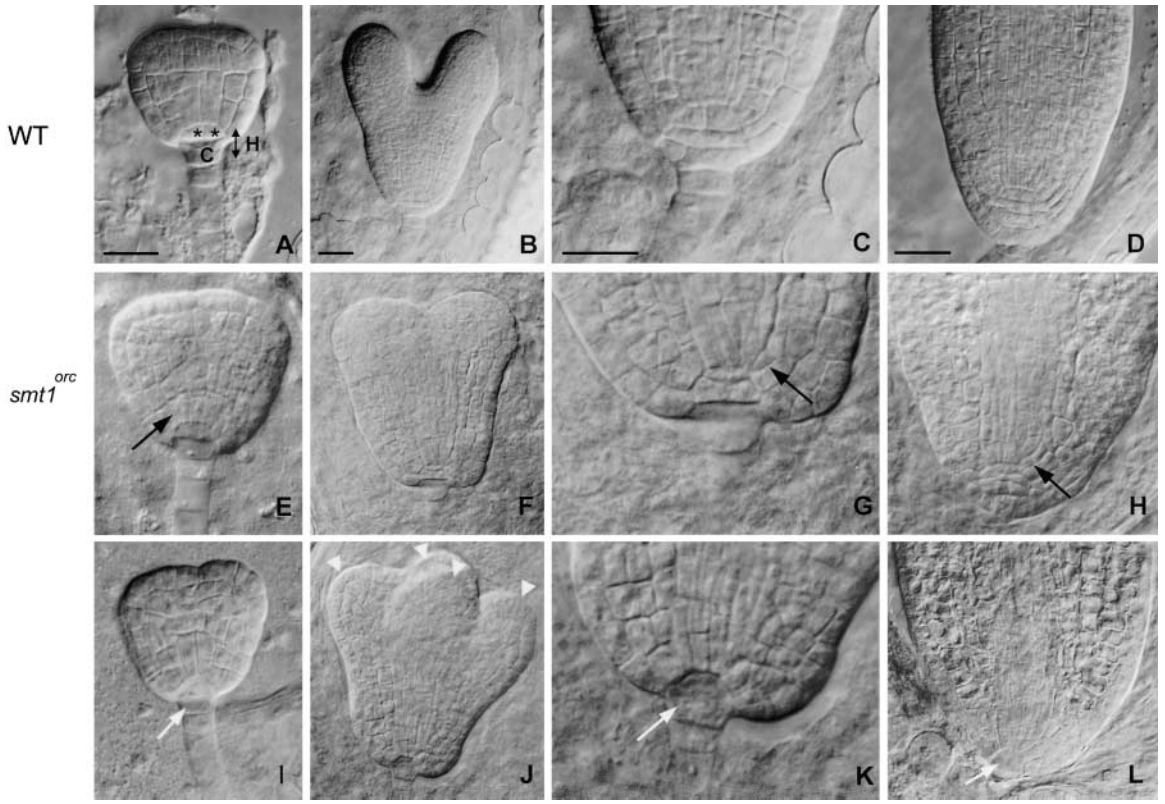

Figure 7. Development of *smt1*^{orc} Embryos.

(A), **(E)**, and **(I)** Globular-stage embryos of the wild type **(A)** and two categories of *smt1*^{orc} **(E)** and **(I)**. Asterisks indicate QC progenitors. C, columella progenitor; H, hypophyseal cell.

(B), **(F)**, and **(J)** Heart-stage embryos of the wild type **(B)** and *smt1*^{orc} **(F)** and **(J)**.

(C) Magnification of **(B)**.

(K) Magnification of **(F)**.

(D), **(H)**, and **(L)** Mature embryos of the wild type **(D)** and *smt1*^{orc} **(H)** and **(L)**.

Embryos were examined under Nomarski optics. Black arrows indicate periclinal divisions in the basal cells of *smt1*^{orc} ground tissue. Arrowheads indicate multiple cotyledon primordia in *smt1*^{orc} embryos. White arrows indicate undivided hypophyseal cells in *smt1*^{orc}. Bars = 25 μm.

DISCUSSION

SMT1 Connects Cell Polarity and Pattern Formation

We have shown that the *SMT1* gene is required for the correct specification of polarity in single cells and for polar auxin transport at the organ level. Misorientation of division planes was observed in early embryos, and trichoblast polarity defects were rescued postembryonically, which suggests that specific cell polarity defects may be the primary consequences of the *smt1*^{orc} mutation. In agreement with these observations, PIN proteins, which are components of the putative auxin efflux machinery, were mislocalized in *smt1*^{orc} mutants, but the AUX1 protein, which is required for auxin influx, was localized cor-

Table 3. Hypophyseal Cell Development in *smt1*^{orc} Embryos

	Wild Type				*smt1*^{orc}			
Stage	Normal Division (%)	Aberrant Division (%)	Undivided (%)	No.	Normal Division (%)	Aberrant Division (%)	Undivided (%)	No.
Early globular	100	0	0	20	33	0	67	18
Triangular	100	0	0	12	61	0	39	28
Heart	100	0	0	71	35	37	28	82
Late heart	100	0	0	24	41	36	22	22

Table 4. *smt1*^{orc} Embryos Display Divisions in the Basal Cell of the Ground Tissue

	Wild Type			*smt1*^{orc}		
Stage	Undivided (%)	Divided (%)	No.	Undivided (%)	Divided (%)	No.
Dermatogen	100	0	12	100	0	12
Early globular	100	0	40	100	0	36
Triangular	100	0	24	98	2	55
Heart	100	0	142	91	9	180
Late heart	100	0	48	81	19	54
Torpedo	100	0	50	73	27	33

rectly. The expression of a synthetic auxin reporter gene, *DR5-GUS*, was changed in *smt1*^{orc} mutants, suggesting profound changes in auxin distribution, and these changes correlated well with observed defects in pattern formation.

Differences in auxin levels have been correlated previously with the patterning of plant embryos (Hadfi et al., 1998), leaf vasculature (Mattsson et al., 1999; Sieburth, 1999), and roots (Sabatini et al., 1999; Friml et al., 2002a). Hence, many, if not all, aspects of the *smt1*^{orc} phenotype may be explained by a primary defect in cell polarity that manifests itself in the multicellular plant by a variety of polar auxin transport defects and their consequences. Differences in sterol composition in *smt1*^{orc} may cause pleiotropic defects unrelated to auxin transport, but most phenotypes observed in *smt1*^{orc} match well with the known functions of *PIN* genes. First, *pin4* embryos show abnormal divisions in the hypophyseal cell and its derivatives, altered *DR5*::*GUS* distribution, increased *DR5*-promoter activity upon auxin treatment, and root-patterning defects (Friml et al., 2002a). Second, cotyledon patterning is affected in *pin1* mutants and upon the application of polar auxin transport inhibitors to embryos (Okada et al., 1991; Liu et al., 1999; Hadfi et al., 1998). Third, clustered xylem elements (vascular islands) were formed in *smt1*^{orc}, which also have been observed after the application of polar auxin transport inhibitors (Mattsson et al.,

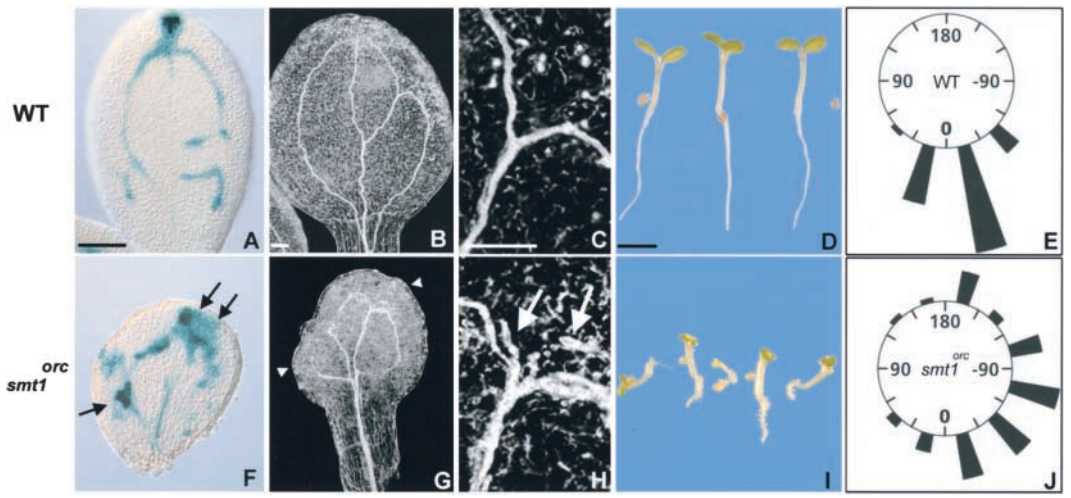

Figure 8. Cotyledon Development and Tropic Responses in *smt1*^{orc}.

(A) *DR5-GUS* expression in a wild-type (WT) mature embryonic cotyledon.
(B) Vascular pattern of a cotyledon of a 5-day-old wild-type seedling.
(C) Enlargement of **(B)**.
(D) Five-day-old seedlings of the wild type.
(E) Scheme of the gravitropic response of wild-type seedling roots after 90° rotation and 24 h in the dark. 0 indicates the direction of the gravity vector after rotation.
(F) Multiple *DR5-GUS* maxima in a *smt1*^{orc} mature embryonic cotyledon (black arrows).
(G) Lobed cotyledon of a 5-day-old *smt1*^{orc} seedling (arrowheads).
(H) Enlargement of **(G)** showing the discontinuous vascular system and the formation of "vascular islands" (white arrows).
(I) Altered tropism in 5-day-old *smt1*^{orc} seedlings.
(J) Gravitropic response of *smt1*^{orc} seedling roots.
(B), **(C)**, **(F)**, and **(G)** show dark-field images of cotyledons of 5-day-old seedlings cleared with chloral hydrate. Bars = 100 μm in **(B)** and **(C)** for **(B)**, **(C)**, **(G)**, and **(H)**, 25 μm in **(A)** for **(A)** and **(F)**, and 2 mm in **(D)** for **(D)** and **(I)**.

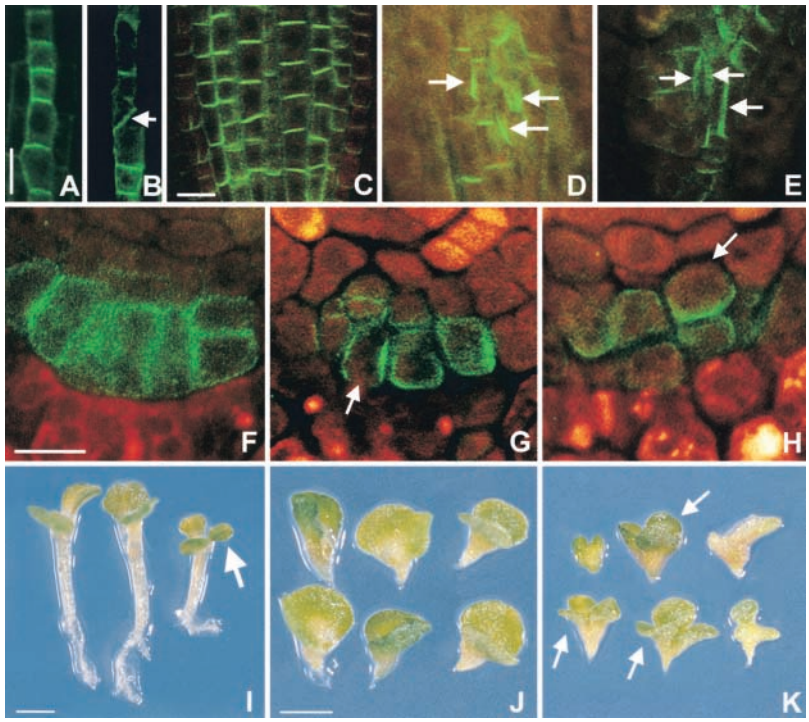

Figure 9. Localization of HA::AUX1 and Delocalized Auxin Efflux Carriers in *smt1*^{orc} and *smt1*^{orc} *gn* Double Mutants.

(A) and **(B)** Immunolocalization of HA::AUX1 at the apical end in protophloem cells of the wild type **(A)** and *smt1*^{orc} **(B)** (arrow indicates an oblique cell wall).

(C) to **(E)** Immunolocalization of PIN1 in the vascular bundle. Expression at the basal end in the central cells in the wild type **(C)** and delocalized expression in vascular cells **(D)** and **(E)** (arrows indicate central, properly axialized *smt1*^{orc} cells).

(F) to **(H)** Immunolocalization of PIN3 in columella cells nearly uniform in the wild type **(F)** and delocalized in *smt1*^{orc} **(G)** and **(H)** (arrows).

(I) to **(K)** *smt1*^{orc} *gn*^{T391} double-mutant analysis.

(I) *smt1*^{orc} seedlings, with multiple cotyledons indicated by the arrow.

(J) *gn*^{T391} seedling.

(K) Additive phenotypes of *smt1*^{orc} *gn*^{T391} double mutants showing slightly smaller seedlings and multiple cotyledons (arrows).

Bars = 10 μm in **(A)**, **(C)**, and **(F)** for **(A)** to **(H)** and 1 mm in **(I)** and **(J)** for **(I)** to **(K)**.

1999). Fourth, the altered gravitropic response of *smt1*^{orc} seedling roots was similar to defects in *pin2* and *pin3* mutants (Luschnig et al., 1998; Müller et al., 1998; Friml et al., 2002b). Thus, the various organ defects in *smt1*^{orc} are strongly similar to defects in mutants and treatments that affect the efflux component of polar auxin transport. Together with the observed differences in the localization of PIN proteins but not AUX1, this finding suggests that defective PIN localization gives rise to many of the phenotypes observed in *smt1*^{orc}.

The altered localization of the nucleus and amyloplasts in columella cells is not readily connected to PIN protein function, which may indicate that PIN proteins are not the only targets of SMT1-mediated cell polarity. PIN1 trafficking has been shown to be actin dependent (Geldner et al., 2001), and actin has been implicated in the localization of the nucleus and the amyloplasts (White and Sack, 1990), but *smt1*^{orc} can respond to cytochalasin B and latrunculin B (data not shown), indicating that the cell polarity defects may not be explained by gross defects in the actin cytoskeleton. Because PIN proteins mark polarity changes but do not necessarily cause them, the nature of other sterol biosynthesis–sensitive targets required for cell polarity remains to be established.

Cell Polarity and Sterol Biosynthesis

It has been shown that the developmental consequences of mutations in sterol biosynthesis are profound (Diener et al., 2000; Schrick et al., 2000, 2002; Carland et al., 2002; Souter et al., 2002). Here, we extend these observations by linking sterol composition to cell polarity. *cvp-1*, *fackel* (*fk*), and *hydra1* (*hyd1*) mutants, which are defective in other enzymes of the sterol biosynthetic pathway, have not been characterized specifically with regard to cell polarity, but reported disturbances in cell division plane orientation (Schrick et al., 2000; Carland et al., 2002) and epidermal morphology (Souter et al., 2002) suggest the presence of polarity defects. However, PIN1 and PIN3 localize normally in *fk/hyd2* and *hyd1* (Souter et al., 2002). Recent evidence shows that a mutation in the yeast homolog ERG6,

which enhances ergosterol levels, leads to the mislocalization of proteins that normally are polarized (Bagnat and Simons, 2002). Perhaps the SMT1-specific side chain modification in the sterol biosynthetic pathway, which is associated with the high accumulation of cholesterol detected only in *smt1* alleles to date, is similarly responsible for defects in protein localization. The lethality of the double mutants *cph fk/hyd2* and *cph hyd1* and different predictions for the localization of the potentially integral membrane proteins FK and HYD1 compared with SMT1 also suggest an independent function of SMT1 (Grebenok et al., 1998; Athenstaedt et al., 1999; Schrick et al., 2000, 2002).

The involvement of vesicle trafficking in PIN protein localization has been deduced from the defective localization of PIN1 observed in *gn* embryos. The *smt1^{orc} gn^{T391}* double-mutant phenotype suggests that *SMT1* can act in the absence of *GN*; hence, it is likely to act in a separate pathway. Furthermore, PIN1 and AUX1 localization are BFA sensitive, suggesting that both proteins are transported by ARF-dependent vesicles (Steinmann et al., 1999; Grebe et al., 2002). Together, the GN independence and the differential effect of the *smt1^{orc}* mutation on PIN1 and AUX1 indicate that sterol biosynthesis does not influence protein localization at the vesicle transport level.

Altered membrane fluidity is a potential explanation for the disturbed distribution of membrane proteins in *smt1^{orc}*. Plant sterol incorporation in human keratinocyte plasma membranes showed that sitosterol, like cholesterol, changed membrane fluidity and permeability (Mora et al., 1999). However, we observed no general smearing but rather discrete alterations in the localization of PIN proteins. Furthermore, preliminary experiments using fluorescence recovery after photobleaching in root hairs did not reveal membrane fluidity differences between *smt1^{orc}* and the wild type (data not shown). Thus, at present, we have no indications that membrane fluidity changes underlie the inappropriate localization of PIN proteins.

Because membrane fluidity appears not to be affected and our double-mutant analysis yielded no evidence for *smt1^{orc}* involvement in vesicle transport, the docking of proteins to specific membrane microdomains, or "lipid rafts," may be affected (Carland et al., 2002). Models have been suggested in which sphingolipid-cholesterol rafts form within the Golgi and sort in a polar fashion to the plasma membrane, possibly using the NSF-SNAP-SNARE protein machinery for docking (Keller and Simons, 1998; Lafont et al., 1998, 1999). Membrane-associated microdomains/rafts are cholesterol dependent (Lang et al., 2001), and future experiments should determine whether AUX1 and PIN localization depends on similar sterol-dependent domains. Specific modulation of sterol biosynthesis through the manipulation of *SMT1* may lead to further insights into the connection between sterols, cell polarity, and differential protein localization in plants.

Table 5. F2 Genotyping of the *smt1^{orc}* × *gn^{T391}* Cross

Genotype	No.	Percent
Wild type	489	57.9
smt1^{orc}	157	18.6
gn	161	19.1
smt1^{orc} gn	37	4.4
Total	844	100

METHODS

Plant Growth Conditions, Plant Strains, and Mutagenesis

The *Arabidopsis thaliana orc* mutant was generated by ethyl methanesulfonate mutagenesis of ecotype Utr (Willemsen et al., 1998). *gn^{T391}* was kindly provided by Gerd Jürgens (Tübingen, Germany). Enhancer trap lines *J2341* and *Q1630*, as described at http://www.plantsci.cam.ac.uk/Haseloff/IndexCatalogue.html, were kindly provided by Jim Haseloff (Cambridge, UK). Promoter trap line QC46 was selected from the Institut National de la Recherche Agronomique T-DNA lines (Bechtold et al., 1993; Sabatini et al., 1999). The *DR5*-β-glucuronidase construct was described by Ulmasov et al. (1997). Homozygous *smt1^{orc}* mutant plants were pollinated with the various mutant, enhancer, and promoter trap lines and analyzed in the homozygous lines of the F3 generation. Seeds were sterilized and plated, and seedlings were grown as described previously by Willemsen et al. (1998). The *smt1^{orc}* mutant was outcrossed twice to ecotype Utr before phenotypic analysis. Outcrossing to Landsberg *erecta*, Columbia, and C24 maintained all aspects of the phenotype, indicating that the Utr ecotype did not contribute to the *orc* phenotype. Whole-mount seedling analysis, embryo studies, and β-glucuronidase assays were performed as described previously (Willemsen et al., 1998).

Map-Based Cloning

Homozygous *orc* plants were crossed to Landsberg *erecta* and Columbia. In the F2 generation, *orc* mutants were selected and DNA was isolated using a cetyl-trimethyl-ammonium bromide method (Lukowitz et al., 1996). We initially mapped the *SMT1* gene to chromosome 5 between markers nga 249 (23.7 centimorgan) and nga 151 (31 centimorgan). Nine hundred zygotic events were used for fine-mapping experiments. Primers were designed using information from the CEREON collection (http://www.arabidopsis.org/) and Primer 3 software (http://www-genome.wi.mit.edu/cgi-bin/primer/primer3_www.cgi/). The interval was narrowed to an interval of 100 kb that was located on three BACs (MSH12, MXE10, and MAC12). Using primers from this region, a transformation-competent artificial chromosome (TAC) vector library (Lui et al., 1993) (obtained from the ABRC Stock Center, Columbus, OH) was screened for overlapping clones in this region. TAC DNA was isolated, electrotransformed into *Agrobacterium tumefaciens* strain C58pMP90, and transformed into homozygous *orc* plants by the floral-dip method (Clough and Bent, 1998). Full complementation was found with TAC K12A16. From TAC K12A16, a HindIII fragment of 8.4 kb spanning open reading frame MSH12.18 (the complete genomic sequence) was isolated and transformed into the pGreen binary vector (Hellens et al., 2000) (http://www.pgreen.ac.uk/) and used for single gene complementation. Total RNA of *smt1^{orc}* seedlings was isolated using the Gentra RNA isolation kit (Biozym, Landgraaf, The Netherlands), c-DNA was isolated using Ready-to-Go beads (Amersham/Pharmacia), and reverse transcriptase–mediated PCR was performed (Ready-to-Go; Amersham/Pharmacia) using primers 5′-CTCCGATTCATCTTTATCCT-3′ (forward) and 5′-GCATGTGCACATGATTCA-3′ (reverse). The genomic and reverse transcriptase–mediated PCR fragments were sequenced using Big Dye Terminator (Genpak Ltd.) on an ABI PRISM 310 genetic analyzer and analyzed using DNASTAR software (Madison, WI).

Sterol Isolation and Quantification

Five-week-old flowering plants were ground in a blender with PBS for 2 min, and total lipid extract was isolated as described previously by Bligh and Dyer (1959). Sterols were purified from the total lipid extract using a silica 200 column. The different fractions were collected and characterized on silica 60 thin layer chromatography plates using phosphorus spray, and the sterol-containing fractions were subjected to gas chromatography–mass spectrometry analysis. Gas chromatography–mass spectrometry was performed under the following conditions: JEOL JMS-AX505W mass spectrometer and Hewlett-Packard 5890 series II gas chromatograph; DB-5MS column (30 m × 0.25 mm; J&W Scientific, Folsom, CA); injection temperature of 260°C; He as carrier gas; flow rate of 1 mL/min; and the following column temperature program: starting temperature of 200°C, increase of 8°C/min to 280°C, and 20 min at 280°C.

Quantification of Cell Polarity Parameters

Amyloplast and nuclear positions were studied in median longitudinal plastic sections prepared as described previously (Scheres et al., 1994, 1995). Amyloplasts were visualized by staining starch on plastic sections using 10% lugol in water and counterstained with 0.05% ruthenium red (Sigma). Only straight cells that aligned with the root axis were used for statistical analysis. The distribution of amyloplasts was determined by dividing the cell length in half to obtain the mid plane and counting the number of amyloplasts that had crossed the mid plane to the apical side. The position of the nucleus was determined as a ratio of the distance from the apical cell wall to the apical edge of the nucleus and the total cell size. Apical-basal hair polarity was determined in trichoblasts of 5-day-old seedlings grown on half-strength germination medium as described by Grebe et al. (2002).

Auxin Application

DR5::*GUS smt1*^{orc} seedlings were grown for 3 days on half-strength germination medium and then transferred to fresh half-strength germination medium agar plates containing 0.5 or 5 μM 2,4-D. After continued growth for another 3 days, GUS expression was visualized.

Polar Auxin Transport Measurements

To standardize the experiment, only the most mature segments of primary wild-type and *smt1*^{orc} inflorescences were taken, which were in contact with the rosette at their basal ends. The apical sites (Figures 4E and 4F, column A) of these segments were loaded with ^{3}H–indoleacetic acid, and transport was allowed during 1.5 h. After transport, the stem sections were cut into three parts: A (apical), B (middle), and C (basal). Then, the amount of auxin transported was measured as described previously by Boot et al. (1999).

Quantification of the Gravitropic Response

Wild-type and *smt1*^{orc} seedlings were grown vertically for 5 days on half-strength germination medium in light and then transferred to fresh half-strength germination medium agar plates in the dark with the root pointing downward. The plates were rotated 90°, and the seedlings continued to grow for another 24 h in the dark. Photographs were taken of the seedlings, and the angle of curvature was determined relative to the bottom (0°).

Immunolocalization

Immunolocalization was performed on whole-mount roots of 5-day-old seedlings as described previously by Gälweiler et al. (1998), Swarup et al. (2001), and Friml et al. (2002a, 2002b).

Upon request, all novel materials described in this article will be made available in a timely manner for noncommercial research purposes.

ACKNOWLEDGMENTS

We thank Ranjan Swarup and Malcolm Bennett for making available seeds of *aux1-22 HA*::*AUX1*; Martijn Koorengevel, Toon de Kroon, and Kees Versluys for technical assistance during sterol measurements and quantification; Jan-Willem Borst for technical assistance during fluorescence recovery after photobleaching experiments; Sabrina Sabatini, Renze Heidstra, Rolf Zeller, and David Welch for critical reading of the manuscript; Frits Kindt, Frouke Kuijer, Ronald Leito, Piet Brouwer, Wil Venendaal, and Pieter van Dorp van Vliet for artwork; and Kees Boot for help with the polar auxin transport measurements. B.S. is supported by a Pionier grant from the Dutch Organization for Sciences, and M.G. is supported by a European Community Marie Curie postdoctoral fellowship (HPMF-CT-2000-0096).

Received October 9, 2002; accepted January 15, 2003.

REFERENCES

Altmann, T. (1998). Recent advances in brassinosteroid molecular genetics. Curr. Opin. Plant Biol. **1,** 378–383.

Athenstaedt, K., Zweytick, D., Jandrositz, A., Kohlwin, S.D., and Daum, G. (1999). Identification and characterization of major lipid particle proteins of the yeast *Saccharomyces cerevisiae*. J. Bacteriol. **181,** 6441–6448.

Bagnat, M., and Simons, K. (2002). Cell surface polarization during yeast mating. Proc. Natl. Acad. Sci. USA **99,** 14183–14188.

Bechtold, N., Ellis, J., and Pelletier, G. (1993). In planta *Agrobacterium*-mediated gene transfer by infiltration of adult *Arabidopsis* plants. C. R. Acad. Sci. Paris **316,** 1194–1199.

Bligh, E.G., and Dyer, W.J. (1959). A rapid method of total lipid extraction and purification. Can. J. Biochem. Physiol. **37,** 91–97.

Boot, K.J.M., van Brussel, A.A.N., Tak, T., Spaink, H.P., and Kijne, J.W. (1999). Lipochitin oligosaccharides from *Rhizobium leguminosarum* bv. *viciae* reduce auxin transport capacity in *Vicia sativa* subsp. *nigra*. Mol. Plant-Microbe Interact. **12,** 839–844.

Brown, D.A., and London, E. (2000). Structure and function of sphingolipid- and cholesterol-rich membrane rafts. J. Cell Biol. **275,** 17221–17224.

Busch, M., Mayer, U., and Jurgens, G. (1996). Molecular analysis of the *Arabidopsis* pattern formation gene *GNOM*: Gene structure and intragenic complementation. Mol. Gen. Genet. **250,** 681–691.

Carland, F.M., Fujioka, S., Takatsuto, S., Yoshido, S., and Nelson, T. (2002). The identification of *CVP1* reveals a role for sterols in vascular patterning. Plant Cell **14,** 2045–2058.

Casimiro, I., Marchant, A., Bhalerao, R.P., Beeckman, T., Dhooge, S., Swarup, R., Graham, N., Inzé, D., Sandberg, G., Casero, P.J., and Bennett M. (2001). Auxin transport promotes Arabidopsis lateral root initiation. Plant Cell **13,** 843–852.

Chen, R., Hilson, P., Sedbrook, J., Rosen, E., Caspar, T., and Masson, P.H. (1998). The *Arabidopsis thaliana AGRAVITROPIC 1* gene encodes a component of the polar-auxin-transport efflux carrier. Proc. Natl. Acad. Sci. USA **95,** 15112–15117.

Clough, S.J., and Bent, A.F. (1998). Floral dip: A simplified method for *Agrobacterium*-mediated transformation of *Arabidopsis thaliana*. Plant J. **16,** 735–743.

Clouse, S., and Feldmann, K. (1999). Molecular genetics of brassinosteroid action. In Brassinosteroids: Steroidal Plant Hormones, A. Sakurai, T. Yokota, and S. Clouse, eds (Tokyo: Springer), pp. 163–190.

Delbarre, A., Muller, P., and Guern, J. (1998). Short-lived and phosphorylated proteins contribute to carrier-mediated efflux, but not to influx, of auxin in suspension-cultured tobacco cells. Plant Physiol. **116,** 833–844.

Delbarre, A., Muller, P., Imhoff, V., and Guern, J. (1996). Comparison of mechanisms controlling uptake and accumulation of 1,4-dichlorophenoxy acetic acid, naphthalene-1-acetic acid, and indole-3-acetic acid in suspension-cultured tobacco cells. Planta **198,** 532–541.

Deyholos, M.K., Cordner, G., Beebe, D., and Sieburth, L.E. (2000). The SCARFACE gene is required for cotyledon and leaf veinpatterning. Development **127,** 3205–3213.

Diener, A.C., Li, H., Zhou, W., Whoriskey, W.J., Nes, W.D., and Fink, G.R. (2000). Sterol methyltransferase 1 controls the level of cholesterol in plants. Plant Cell **12,** 853–870.

Dolan, L., Janmaat, K., Willemsen, V., Linstead, P., Poethig, S., Roberts, R., and Scheres, B. (1993). Cellular organisation of the *Arabidopsis thaliana* root. Development **119,** 71–84.

Estelle, M. (1998). Polar auxin transport: New support for an old model. Plant Cell **10,** 1775–1778.

Friml, J., Benkova, E., Blilou, I., Wisniewska, J., Hamann, T., Ljung, K., Woody, S., Sandberg, G., Scheres, B., Jürgens, G., and Palme, K. (2002a). AtPIN4 mediates sink-driven auxin gradients and root patterning in *Arabidopsis*. Cell **108,** 661–673.

Friml, J., Wisniewska, J., Benkova, E., Mendgen, K., and Palme, K. (2002b). Lateral relocation of auxin efflux regulator PIN3 mediates tropism in *Arabidopsis*. Nature **415,** 806–809.

Gälweiler, L., Guan, C., Muller, A., Wisman, E., Mendgen, K., Yephremov, A., and Palme, K. (1998). Regulation of polar auxin transport by AtPIN1 in *Arabidopsis* vascular tissue. Science **282,** 2226–2230.

Geldner, N., Friml, J., Stierhof, Y.D., Jürgens, G., and Palme, K. (2001). Auxin transport inhibitors block PIN1 cycling and vesicle trafficking. Nature **413,** 425–428.

Grebe, M., Friml, J., Swarup, R., Ljung, K., Sandberg, G., Terlou, M., Palme, K., Bennett, M.J., and Scheres, B. (2002). Cell polarity signaling in *Arabidopsis* involves a BFA-sensitive auxin influx pathway. Curr. Biol. **12,** 329–334.

Grebenok, R.J., Ohnmeiss, T.E., Yamamoto, A., Huntley, E.D., Galbraith, D.W., and Della Penna, D. (1998). Isolation and characterization of an *Arabidopsis thaliana* C-8,7 sterol isomerase: Functional and structural similarities to mammalian C-8,7 sterol isomerase/emopamil-binding protein. Plant Mol. Biol. **38,** 807–815.

Hadfi, K., Speth, V., and Neuhaus, G. (1998). Auxin-induced developmental patterns in *Brassica juncea* embryos. Development **125,** 879–887.

Hellens, R.P., Edwards, E.A., Leyland, N.R., Bean, S., and Mullineaux, P.M. (2000). pGreen: A versatile and flexible binary Ti vector for Agrobacterium-mediated plant transformation. Plant Mol. Biol. **42,** 819–832.

Hertel, R., Lomax, T.L., and Briggs, W.R. (1983). Auxin transport in membrane vesicles from *Cucurbita pepo* L. Planta **157,** 193–201.

Heyn, A., Hoffmann, S., and Hertel, R. (1987). In vitro auxin transport in membrane vesicles from maize coleoptiles. Planta **172,** 285–287.

Keller, P., and Simons, K. (1998). Cholesterol is required for surface transport of influenza virus hemagglutinin. J. Cell Biol. **140,** 1357–1367.

Knoblich, J.A. (2001). Asymmetric cell division during animal development. Nat. Rev. Mol. Cell. Biol. **2,** 11–20.

Lafont, F., Lecat, S., Verkade, P., and Simons, K. (1998). Annexin XIIIb associates with lipid microdomains to function in apical delivery. J. Cell Biol. **142,** 1413–1427.

Lafont, F., Verkade, P., Galli, T., Wimmer, C., Louvard, D., and Simons, K. (1999). Raft association of SNAP receptors acting in apical trafficking in Madin-Darby canine kidney cells. Proc. Natl. Acad. Sci. USA **96,** 3734–3738.

Lang, T., Bruns, D., Wenzel, D., Riedel, D., Holroyd, P., Thiele, C., and Jahn, R. (2001). SNAREs are concentrated in cholesterol-dependent clusters that define docking and fusion sites for exocytosis. EMBO J. **20,** 2202–2213.

Liu, Y., Shirano, Y., Fukaki, H., Yanai, Y., Tasaka, M., Tabata, S., and Shibata, D. (1999). Complementation of plant mutants with large genomic DNA fragments by a transformation-competent artificial chromosome vector accelerates positional cloning. Proc. Natl. Acad. Sci. USA **96,** 6535–6540.

Lui, C.-M., Xu, Z.-H., and Chua, N.-H. (1993). Auxin polar transport is essential for the establishment of bilateral symmetry during early plant embryogenesis. Plant Cell **5,** 621–630.

Lukowitz, W., Mayer, U., and Jürgens, G. (1996). Cytokinesis in the *Arabidopsis* embryo involves the syntaxin-related *KNOLLE* gene product. Cell **84,** 61–71.

Luschnig, C., Gaxiola, R.A., Grisafi, P., and Fink, G.R. (1998). EIR1, a root-specific protein involved in auxin transport, is required for gravitropism in *Arabidopsis thaliana*. Genes Dev. **12,** 2175–2187.

MacCleery, S.A., and Kiss, J.Z. (1999). Plastid sedimentation kinetics in roots of wild-type and starch-deficient mutants of *Arabidopsis*. Plant Physiol. **120,** 183–192.

Marchant, A., Kargul, J., May, S.T., Muller, P., Delbarre, A., Perot-Rechenmann, C., and Bennett, M.J. (1999). AUX1 regulates root gravitropism in *Arabidopsis* by facilitating auxin uptake within the root apical tissues. EMBO J. **18,** 2066–2073.

Massucci, J.D., and Schiefelbein, J.W. (1994). The *rhd6* mutation of *Arabidopsis thaliana* alters root hair initiation through an auxin- and ethylene-associated process. Plant Physiol. **106,** 1335–1346.

Mattsson, J., Sung, Z.R., and Berleth, T. (1999). Responses of plant vascular systems to auxin transport inhibition. Development **126,** 2979–2991.

Mayer, U., Büttner, G., and Jürgens, G. (1993). Apical-basal pattern formation in the *Arabidopsis* embryo: Studies on the role of the *GNOM* gene. Development **117,** 149–162.

Mora, M.P., Tourne-Peteilh, C., Charveron, M., Fabre, B., Milon, A., and Muller, I. (1999). Optimisation of plant sterols incorporation in human keratinocyte plasma membrane and modulation of membrane fluidity. Chem. Phys. Lipids **101,** 255–265.

Morris, D.A., and Robinson, J.S. (1998). Targeting of auxin carriers to the plasma membrane: Differential effects of brefeldin A on the traffic and auxin uptake of efflux carriers. Planta **205,** 606–612.

Mossessova, E., Gulbis, J.M., and Goldberg, J. (1998). Structure of the guanine nucleotide exchange factor sec 7 domain of human ARNO and analysis of the interaction with ARF GTPase. Cell **92,** 415–423.

Müller, A., Guan, C., Gälweiler, L., Tänzler, P., Huijser, P., Marchant, A., Parry, G., Bennett, M., Wisman, E., and Palme, K. (1998). AtPIN2 defines a locus of *Arabidopsis* for root gravitropism control. EMBO **17,** 6903–6911.

Okada, K., Ueda, J., Kornake, M.K., Bell, C.J., and Shimura, Y. (1991). Requirement of the auxin polar transport system in early stages of *Arabidopsis* floral bud formation. Plant Cell **3,** 677–684.

Patterson, M.C., Di Bisceglie, A.M., Higgins, J.J., Abel, R.B.,

Schiffmann, R., Parker, C.C., Argoff, C.E., Grewal, R.P., Yu, K., and Pentchev, P.G. (1993). The effect of cholesterol-lowering agents on hepatic and plasma cholesterol in Niemann-Pick disease type C. Neurology **43,** 61–64.

Przemeck, G.K.H., Mattsson, J., Hardtke, C.S., Sung, A.R., and Berleth, T. (1996). Studies on the role of the Arabidopsis gene MONOPTEROS in vascular development and plant axialization. Planta **200,** 229–237.

Rahman, A., Ahamed, A., Amakwa, T., Goto, N., and Tsurumi, S. (2001). Chromosaponin I specifically interacts with AUX1 protein in regulating the gravitropic response of *Arabidopsis* roots. Plant Physiol. **125,** 990–1000.

Rodriguez-Boulan, E., and Nelson, W.J. (1989). Morphogenesis of the polarized epithelial cell phenotype. Science **245,** 718–725.

Sabatini, S., Beis, D., Wolkenfelt, H., Murfett, J., Guilfoyle, T., Malamy, J., Benfey, P., Leyser, O., Bechtold, N., Weisbeek, P., and Scheres, B. (1999). An auxin-dependent distal organizer of pattern and polarity in the *Arabidopsis* root. Cell **99,** 463–472.

Scheres, B., DiLaurenzio, L., Willemsen, V., Hauser, M.-T., Janmaat, K., Weisbeek, P., and Benfey, P. (1995). Mutations affecting the radial organisation of the *Arabidopsis* root display specific defects throughout the embryonic axis. Development **121,** 53–62.

Scheres, B., McKhann, H., van den Berg, C., Willemsen, V., Wolkenfelt, H., de Vrieze, G., and Weisbeek, P. (1996). Experimental and genetic analysis of root development in *Arabidopsis thaliana*. Plant Soil **187,** 97–105.

Scheres, B., Wolkenfelt, H., Willemsen, V., Terlouw, M., Lawson, E., Dean, C., and Weisbeek, P. (1994). Embryonic origin of the *Arabidopsis* primary root and root meristem initials. Development **120,** 2475–2487.

Schrick, K., Mayer, U., Horrichs, A., Kuhnt, C., Bellini, C., Dangl, J., Schmidt, J., and Jürgens, G. (2000). FACKEL is a sterol C-14 reductase required for organized cell division and expansion in *Arabidopsis* embryogenesis. Genes Dev. **14,** 1471–1484.

Schrick, K., Mayer, U., Martin, G., Bellini, C., Kuhnt, C., Schmidt, J., and Jürgens, G. (2002). Interactions between sterol biosynthesis genes in embryonic development of *Arabidopsis*. Plant J. **30,** 61–73.

Sieburth, L. (1999). Auxin is required for leaf vein pattern in *Arabidopsis*. Plant Physiol. **121,** 1179–1190.

Souter, M., Topping, J., Pullen, M., Friml, J., Palme, K., Hackett, R., Grierson, D., and Lindsey, K. (2002). *hydra* mutants of Arabidopsis are defective in sterol profiles and auxin and ethylene signaling. Plant Cell **14,** 1017–1031.

Steinmann, T., Geldner, N., Grebe, M., Mangold, S., Jackson, C.L., Paris, S., Gälweiler, L., Palme, K., and Jürgens, G. (1999). Coordinated polar localization of auxin efflux carrier PIN1 by GNOM ARF GEF. Science **286,** 316–318.

Swarup, R., Friml, J., Marchant, A., Ljung, K., Sandberg, G., Palme, K., and Bennett, M. (2001). Localization of the auxin permease AUX1 suggests two functionally distinct hormone transport pathways operate in the *Arabidopsis* root apex. Genes Dev. **15,** 2648–2653.

Ulmasov, T., Murfett, J., Hagen, G., and Guilfoyle, T.J. (1997). Aux/IAA proteins repress expression of reporter genes containing natural and highly active synthetic auxin response elements. Plant Cell **9,** 1963–1971.

van den Berg, C., Willemsen, V., Hendriks, G., Weisbeek, P., and Scheres, B. (1997). Short-range control of cell differentiation in the *Arabidopsis* root meristem. Nature **390,** 287–289.

Vroemen, C.W., Langeveld, S., Mayer, U., Ripper, G., Jürgens, G., van Kammen, A., and de Vries, S.C. (1996). Pattern formation in the Arabidopsis embryo revealed by position-specific lipid transfer protein gene expression. Plant Cell **8,** 783–791.

White, R.G., and Sack, F.D. (1990). Actin microfilaments in presumptive statocytes of root cap and coleoptiles. Am. J. Bot. **77,** 17–26.

Willemsen, V., Wolkenfelt, H., de Vrieze, G., Weisbeek, P., and Scheres, B. (1998). The *HOBBIT* gene is required for formation of the root meristem in the *Arabidopsis* embryo. Development **125,** 521–531.